Study on Landslide Orientation Bias Triggered by 1994 Northridge Earthquake

by

Hiroshi P. Sato[1]

ABSTRACT

Previous studies reported that the 1994 Northridge earthquake triggered 11,000 landslides in 10,000 km^2; however, no study has investigated the landslide orientation bias in the wider area than the Santa Susana quadrangle map, i.e., 124 km^2. I selected 3,200 km^2 on the mountain slope and found that the bias shows the direction from south to west. I also investigated the relation between the landslide slope orientation and ground acceleration direction of initial and peak sliding acceleration (ISA and PSA), using simulated horizontal and vertical ground acceleration data. As a result, it was found that PSA gives better explanation than ISA for the landslide orientation bias of southwest; however, since north-facing slopes also showed the highest accumulated PSA, I could not state the reason why many landslides did not occur on the north-facing slopes.

KEYWORDS: Aspect, California, Ground Acceleration, Landslide, Northridge Earthquake, Slope

1. INTRODUCTION

On 17 January 1994, Northridge earthquake (Mw 6.7) occurred 18 km beneath the Northridge, Southern California [1], neighborhood in the city of Los Angeles. The earthquake resulted from more than 3 m of reverse slip on a 15-km-long south-dipping thrust fault that raised the Santa Susana Mountains by as much as 70 cm [2].

Northridge earthquake triggered 11,000 landslides over 10,000 km^2 [3][4]. They described that deep landslide was rare and almost all of the landslides were shallow disrupted rock slide, and tell that the landslides were concentrated primarily in the Santa Susana Mountains and the mountains north of the Santa Clara River Valley. Since no rain had fallen for several month before the earthquake; hence, pore-pressure effect were not a factor in triggering landslides [3][4].

Harp and Jibson [3][4] also reported that the earthquake induced-landslide were concentrated more on south (S)- than north (N)- slope aspect (the direction which the slope faces) in Santa Susana Mountains. Parise and Jibson [5] also said that the landslides have Southeast (SE)~Southwest (SW) orientation bias in the 124 km^2 area using 10-m-resolution digital elevation model (DEM) prepared by U.S. Geological Survey (USGS).

Such the bias was also shown in the other cases of earthquakes; e.g., the bias of SW [6] in the 2005 Northern Pakistan earthquake (M7.6), the bias of S [7] in the 1999 Chi-Chi earthquake (Mw 7.6) in Taiwan, and the bias of SE [7] in the 1993 earthquake (Mw 6.9) in Finisterre Mountain, Papua New Guinea. It is thought that the relation between slope aspect and ground acceleration direction has close relation to trigger landslides. However, previous studies have not investigated the relation between them enough.

Time-series ground acceleration shows different directions in each measurement time, and slope aspect is variable among the different sites. Furthermore, steep slope angle is an important factor to induce landslides. Since time-series sliding acceleration [8] in each site is also calculated from the ground acceleration, I investigated the relation between slope aspect and the time-series sliding acceleration, inducing landslides.

2. STUDY AREA

[1] Senior Researcher, Geography and Crustal Dynamics Research Center, Geographical Survey Institute, Tsukuba-shi, Ibaraki-ken 305-0811 Japan

2.1 Topography

Study area is shown in Fig.1a, where elevation ranges from 0 m, at the coast facing Pacific Ocean, to the summit 2,248 m at the site A. Figure 1a also depicts the model fault plane [9] whose upper edge is shown as D. The position B-B' in Fig. 1a shows the Susana Mountains.

Figure 1b shows the mapped landslides [3][4] as red dots. The site C in Fig.1a shows Simi Hills where Cretaceous hard sandstone lies, and the landslide density in the Simi Hills was smaller than in Santa Susana Mountains [3][4][5]. Figures 1c and 1d depict slope angle and aspect calculated from 40-m-resolution DEM. In this study I deal landslides occurred on mountain slope, therefore, I limited the study area where slope angle is 5º and more; Figures 1c and 1d shows just the area, 3,200 km^2. Furthermore, I selected the landslide whose area is more than 40 m by 40 m, this is because I thought that large landslides clearly shows their orientation (the directions that the landslides face on the slopes).

2.2 Landslide Orientation Bias

I overlaid the slope aspect in Fig.1d on the mapped landslides in Fig.1b; I calculated the landslide area ratio among eight orientations. As a result, the radar chart in Fig.2a showed the SW orientation bias.

To confirm slope steepness effect on the bias, I overlaid the slope angle in Fig.1c on the mapped landslides; I calculated the average slope angle among eight orientations. As a result, Fig.2b does not show remarkable slope angle changes among them and it means that slope steepness does not control the landslide orientation bias in the whole study area.

Next, to confirm geologic unit effect on the bias, I overlaid the geologic map [10] on the mapped landslides; I calculated the landslide area ratio among both eight orientations and the 18 kinds of geologic unit, from Pre-Cambrian granite to Holocene sediments. All units except Miocene continental sedimentary rocks showed S, SW, and west (W) orientation bias and it means that geologic unit does not control the landslide orientation bias in the whole study area.

3. METHOD

3.1 Simulated Ground Acceleration Data

Jibson and Jibson [11] showed the 84 seismometer instruments in and around the study area. I drew the instrument-centered 2-km-radius sampling circles on the landslide polygons; however, almost all of the sampling circles did not have the enough numbers of landslide polygon because the instruments are not always installed in the mountains. Only the four instruments of FSD, WPI, PDD, and PDA in Fig.1c (PDA is in the same place as PDD) showed over 1% landslide area ratio in each sampling circle.

However, the number of the sampling circles is not enough to consider landslide orientation bias in the whole study area. Therefore, in this study I did not use the real ground acceleration data [11] but I used the simulated ground acceleration data at the 4-km-spacing 144 sites, from the site #1 to #144. The data have northing, easting, and up components and whose sampling time and period is 0.04 second and 50 seconds, respectively. Since the simulated data [12] originally provides ground velocity, I calculated the acceleration from the velocity data. In calculating the velocity Wald et al. [12] considered substrate stiffness differences between hard and soft rock; however, they did not consider topographic seismic-wave amplification effect; hence, calculated acceleration does not contain this effect.

On the mapped landslides I overlaid 2-km-radus sampling circles whose centers are the 144 sites, and I investigated landslide area ratio within the sampling circles. As a result, I selected 12 sampling circles where the landslide area ratio is over 1%. Figure 1d shows these 12 sampling circles of #64, #65, #76~#78, #81, #89, #98~#101, and #112. Within the 12 sampling circles I overlaid the slope aspect on the mapped landslides, calculated 2,072 landslide DEM cells number ratio among eight orientations (Fig.3a). Again, I could find the S~SW orientation bias.

Figure 3b shows the whole DEM cells distribution ratio in the 12 sampling circles; however, no orientation bias was found in the radar chart.

3.2 Sliding acceleration calculation

In this study we assumed that any DEM cells in each sampling circle have the same ground acceleration. In each sampling circle I calculated sliding acceleration [8] using the simulated ground acceleration data. As an example, at the DEM cell (SW slope aspect in a landslide polygon, within the sampling circle #77), I show the easting a_E, northing a_N, and up a_V components of the ground acceleration in Figs.4a, 4b, and 4c, respectively.

For calculating sliding acceleration, in Fig.5 Huang et al. [8] assumed free landslide body whose mass is m on the basement. Relative to the inertial frame of reference, the basement moves with acceleration a_n in the direction of normal to the slide surface (positive away from the slope), a_d tangential to the slide surface along the dip (positive down dip), and a_s tangential to the slide surface along the strike. In Fig.5, a_s is not written because it is vertical to the page (positive up-away from the page). Eqs.(1) and (2) shows how to calculate a_n and a_d [8].

$$a_n = a_E \sin\delta\cos\varphi_s - a_N \sin\delta\sin\varphi_s + a_V \cos\delta \quad (1)$$

$$a_d = a_E \cos\delta\cos\varphi_s - a_N \cos\delta\sin\varphi_s - a_V \sin\delta \quad (2)$$

Where, δ and φ_s is slope angle and slope strike direction from north measured clockwise, which is equal to slope aspect minus 90°, respectively. The a_n and a_d calculated from a_E, a_N, and a_V is shown in Figs.4d and 4e.

Finally, sliding acceleration S_a was calculated by Eq.(3). The S_a calculated from a_n and a_d is shown in Fig.4f. If S_a is positive, it will move the slope surface; if not, the surface will stay.

$$S_a = (g\sin\delta - a_d) - \mu_s(g\cos\delta + a_n) - c'/mA \quad (3)$$

Where, g, δ, μ_s, c', A is gravity, slope angle, the coefficient of static friction, effective cohesive strength across the sliding surface, and area of the sliding surface, respectively. The coefficient of static friction μ_s was calculated from $\mu_s = \tan(\varphi')$, where φ' is effective friction angle. The values of φ' and c' in each geologic unit [10] were determined by Jibson et al. [13] referring to the lithologic facies of the geologic units.

3.3 Initial and Peak Sliding Acceleration (ISA and PSA) Selection

Time-series sliding acceleration was calculated at each DEM cells, whose number is 2,072 landslide cells and 54,289 no-landslide cells. In each DEM cell slope aspect was calculated. If original a_E and a_N in Figs.4b and 4c are referred to, I can calculate the ground acceleration direction from a_E and a_N in any time in Fig.4f. Therefore, in each cell I selected the two kinds of positive sliding acceleration and compared slope aspects with ground acceleration direction in each case.

First, I selected the ISA that moves slope surface for the first time; e.g., in Fig.4f, initial positive S_a is 0.03 m/s/s and the recorded time is 4.84 second. This is because I expected that ground acceleration direction of ISA would determine the landslide orientation. Next, I extracted PSA; e.g., in Fig.4f, PSA is 0.99 m/s/s and the recorded time is 8.72 second. This is because I thought that ISA may be small to move slope surface in practice and PSA is effectively working to move it. In the both cases, I recorded not only the ISA and PSA but also whose original ground acceleration direction at the time and slope aspect at the cell.

However, in the two cases, it is not efficient to consider the relation between the slope aspect and ground acceleration direction at each DEM cell, because the number of DEM cells is totally 56,361; therefore, I accumulated the ISA and PSA among the slope aspect and ground acceleration directions in the whole sampling circle.

4. RESULTS

4.1 Initial Sliding Acceleration (ISA)

Figure 6a shows the accumulated ISAs at 2,072 landslide DEM cells among slope aspects and ground acceleration directions. Generally speaking, high accumulated ISAs are concentrated on and around the diagonal line between slope aspect N, ground acceleration direction S and slope aspect NW, ground acceleration direction SE. The highest accumulated ISA recorded 19.3 m/s/s in the slope aspect SW, ground acceleration direction NE. The fourth highest accumulated ISA recorded 10.0 m/s/s in the slope aspect N, ground acceleration direction S. Since the landslide DEM cells face more SW than N (Fig.2a), I thought that more ISAs were accumulated on the SW-facing DEM than on the N-facing DEM.

Figure 6b shows the accumulated ISAs at both 2,072 landslide DEM cells and 54,289 no-landslide DEM cells, i.e., at the all 56,361 DEM cells within the whole sampling area. The highest accumulated ISA recorded 138.6 m/s/s in the slope aspect N, ground acceleration direction S. The second highest accumulated ISA recorded 84.3 m/s/s in the slope aspect SW, ground acceleration direction NE. And it looks like two peaks of accumulated ISA around the slope aspect N, ground acceleration S, and slope aspect SW, ground acceleration NE.

To normalize Fig.6a, I divided Fig.6a by Fig.6b. The result is shown in Fig.6c; it shows 100% in the slope aspect SW, ground acceleration direction SW, and in the slope aspect W, ground acceleration direction S. Furthermore, 99.4% recorded in the slope aspect N, ground acceleration direction NW; however, Fig.6c does not show that higher accumulated ISAs were added on the landslide SW-facing slope, regardless of ground acceleration direction.

4.2 Peak Sliding Acceleration (PSA)

Figure 6d shows the accumulated PSA at 2,072 landslide DEM cells among slope aspects and ground acceleration directions. The highest accumulated PSA recorded 83.3 m/s/s in the slope aspect SW, ground acceleration direction NE. The seventh highest accumulated PSA recorded 40.0 m/s/s in the slope aspect N, ground acceleration direction S.

Figure 6e shows the accumulated PSAs at the all 56,361 DEM cells. The highest accumulated PSA recorded 341.4 m/s/s in the slope aspect N, ground acceleration direction S. The second highest accumulated PSA recorded 289.2 m/s/s in the slope aspect SW, ground acceleration direction NE. And it also shows two peaks of accumulated PSA around the first and second highest accumulated PSA.

Figure 6f shows the normalized accumulated PSA by dividing Fig.6d by Fig.6e; it was found that the slope aspect SW tended to experience relatively higher ratio than the other slope aspects, regardless of ground acceleration direction. Comparing Fig.6f with Fig.3a, I found that landslide orientation bias is closely related with the normalized accumulated PSA among the slope aspects. However, if we focus on the slope aspect N and SW in Fig.6e, we cannot state the reason why landslides did not occur at the slope aspect of N.

5. CONCLUSIONS

In this study I revealed that the 1994 Northridge earthquake-induced landslides have the orientation bias of SW over the whole mountain area, 3,200 km^2. Next, I stated that the bias is not controlled by the slope steepness and geologic units. I also stated that PSA (peak sliding acceleration) gives better explanation than ISA (initial sliding acceleration) for the SW landslide orientation bias. However, we could not state the reason why landslides did not occur at the N-facing slope where the highest accumulated PSA recorded in Fig.6e.

6. ACKNOWLEDGEMENT

Support for my research at the U.S. Geological Survey facilities in Golden, CO was provided by a grant from the Ministry of Education, Culture, Sports, Science and Technology of Japan.

7. REFERENCES

1. Wald, D.J., Heaton, T.H.: A Dislocation of the 1994 Northridge, California Earthquake

Determined from Strong Ground Motions, *U.S. Geological Survey Open-File Report*, No. 94-278, 1996.
2. U.S. Geological Survey and the Southern California Earthquake Center: The Magnitude 6.7 Northridge, California, earthquake of January 17, 1994, *Science*, Vol.266, 389-397, 1994.
3. Harp, E.L., Jibson, R.W.: Inventory of landslides triggered by the 1994 Northridge, California earthquake, *U.S. Geological Survey Open-File Report*, No. 95-213, 1995.
4. Harp, E.L., Jibson, R.W.: Landslides triggered by the 1994 Northridge, California earthquake, *Bulletin of the Seismological Society of America*, Vol.86(1B), S319-S332, 1996.
5. Parise, M., Jibson, R.W.: A Seismic Landslide Susceptibility Rating of Geologic Units based on Analysis of Characteristics of Landslides Triggered by the 17 January, 1994 Northridge, California Earthquake, *Engineering Geology*, Vol.58, 251-270, 2000.
6. Sato, H.P., Hasegawa, H., Fujiwara, S., Tobita, M., Koarai, M., Une, H., Iwahashi, J.: Interpretation of Landslide Distribution Triggered by the 2005 Northern Pakistan Earthquake using SPOT5 Imagery, *Landslides*, Vol.4, 113-122, 2007.
7. Meunier, P., Houvius, N., Haines, J.A.: Topographic Site Effects and the Location of Earthquake Induced Landslides, *Earth Planetary Science Letters*, Vol.275, 221-232, 2007.
8. Huang, C.C., Lee, Y.H., Liu, H.P., Keefer, D.K., Jibson, R.W.: Influence of Surface-Normal Ground Acceleration on the Initiation of Jih-Feng-Erh-Shan Landslide During the 1999 Chi-Chi, Taiwan, Earthquake, *Bulletin of the Seismological Society of America*, Vol.91, 953-958, 2001.
9. Wald, D.J., Heaton, T.H., Hudnut, K.W.: The Slip History of the 1994 Northridge, California, Earthquake Determined from Strong-motion, Teleseismic, GPS, and Leveling Data, *Bulletin of the Seismological Society of America*, Vol.86(1B), S49-S70, 1996.
10. Jennings, C.W.: Geologic Map of California (Scale 1:750,000), State of California, 1977.
11. Jibson, R.W., Jibson, M.W.: Java Programs for Using Newmark's Method and Simplified Decoupled Analysis to Model Slope Performance During Earthquakes, *U.S. Geological Survey Open-File Report*, No.03-005, 2003.
12. Wald, D.J., Hudnut, K.W., Heaton, T.H.: Estimation of Uniformly Spaced, Near-source, Broadband Ground Motions for the 1994 Northridge Earthquake from Forward and Inverse Modeling, *Proceedings of the CUREe Northridge Earthquake Research Conference, Los Angeles*, 1997. (http://pasadena.wr.usgs.gov/office/wald/CUREe.html)
13. Jibson, R.W., Harp, E.L., Michael, J.A.: A Method for Producing Digital Probabilistic Seismic Landslide Hazard Maps: an Example from the Los Angels, California, Area, *U.S. Geological Survey Open-File Report*, No.98-113, 1998.

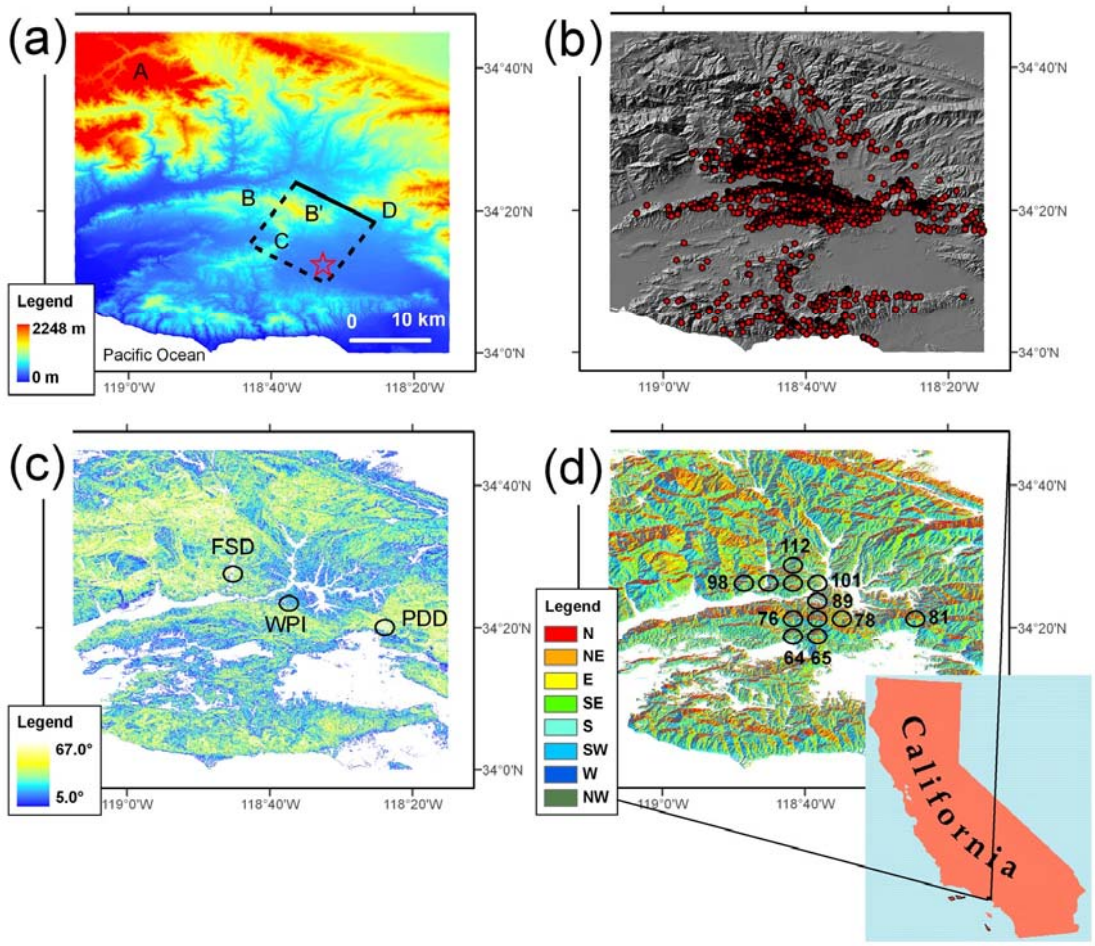

Fig.1 Study Area

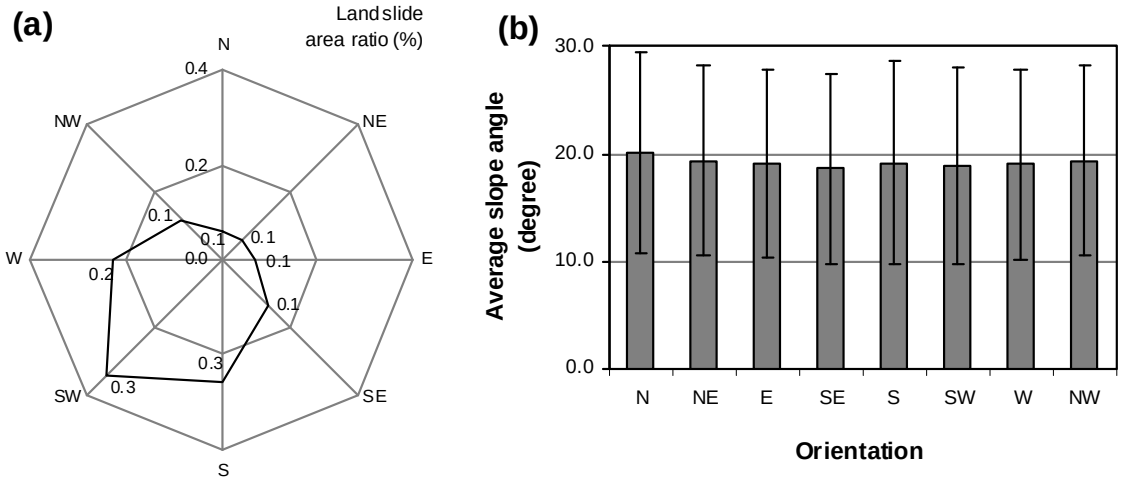

Fig.2 (a) Landslide Area Ratio among Eight Orientations and (b) Average Slope Angle (Error Bar Means Standard Deviation) among Eight Orientations in the Whole Study Area

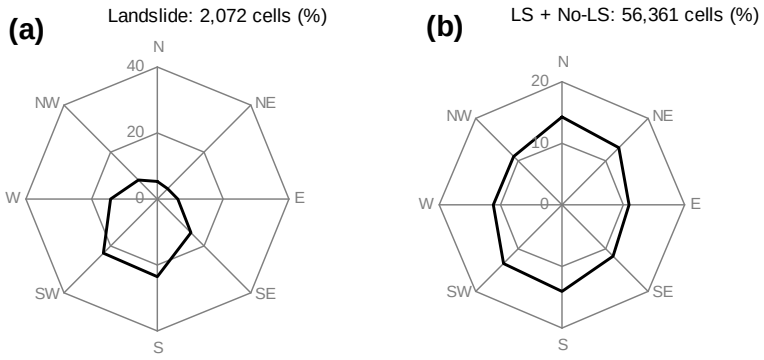

Fig.3 Orientation Ratio in (a) 2,072 Landslide Cells, (b) Whole Cells (2,072 Landslide Cells + 54,289 No-landslide Cells)

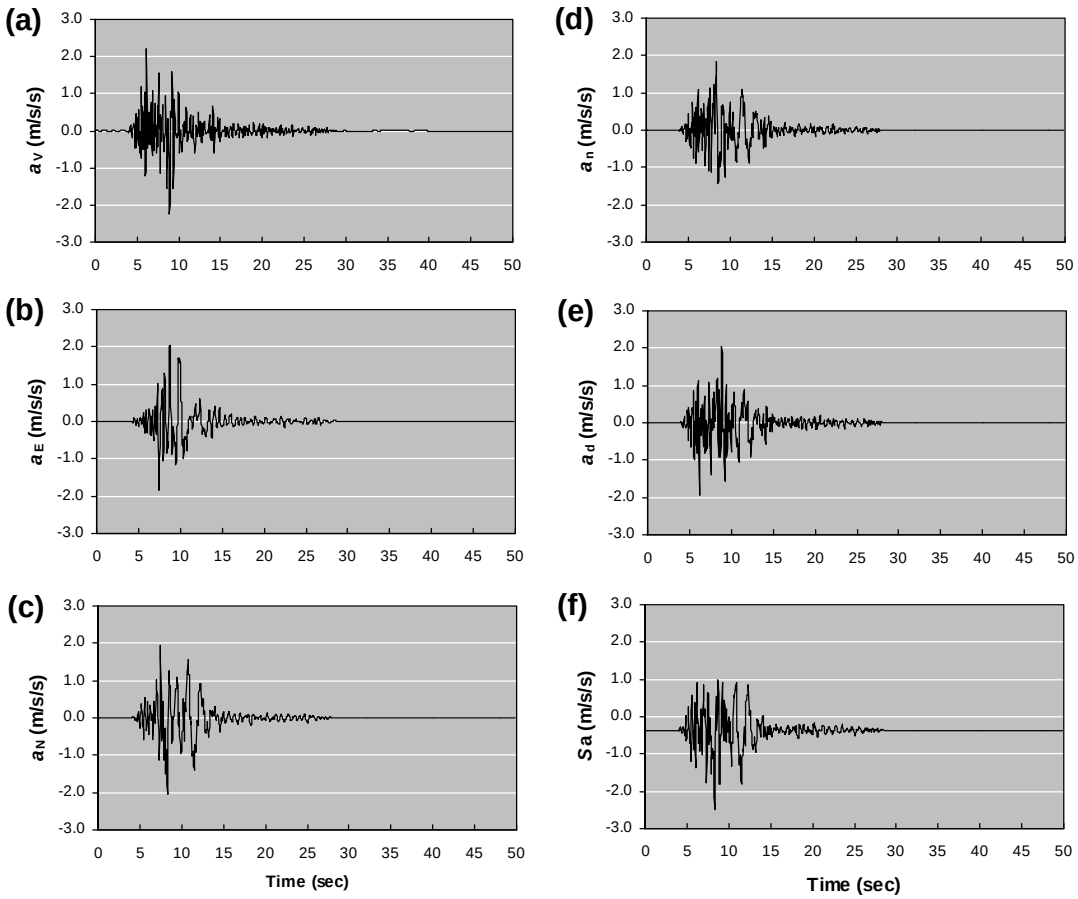

Fig.4 (a), (b), and (c) are the Examples of Ground Acceleration, Up (a_v), Easting (a_E), and Northing (a_N) Component, Respectively at the Cell (Slope Angle and Slope Aspect is 53.8° and 206.6°, Respectively) in the Sampling Circle #77 (in Fig.1d). Ground Acceleration a_d in Tangential to the Slide Surface along the Dip (Positive Down Dip) shows (d), and (e) is a_n in the Direction of Normal to the Slide Surface (Positive Away from the Slope) in Landslide Area. The (f) is Sliding Acceleration Calculated from a_n and a_d.

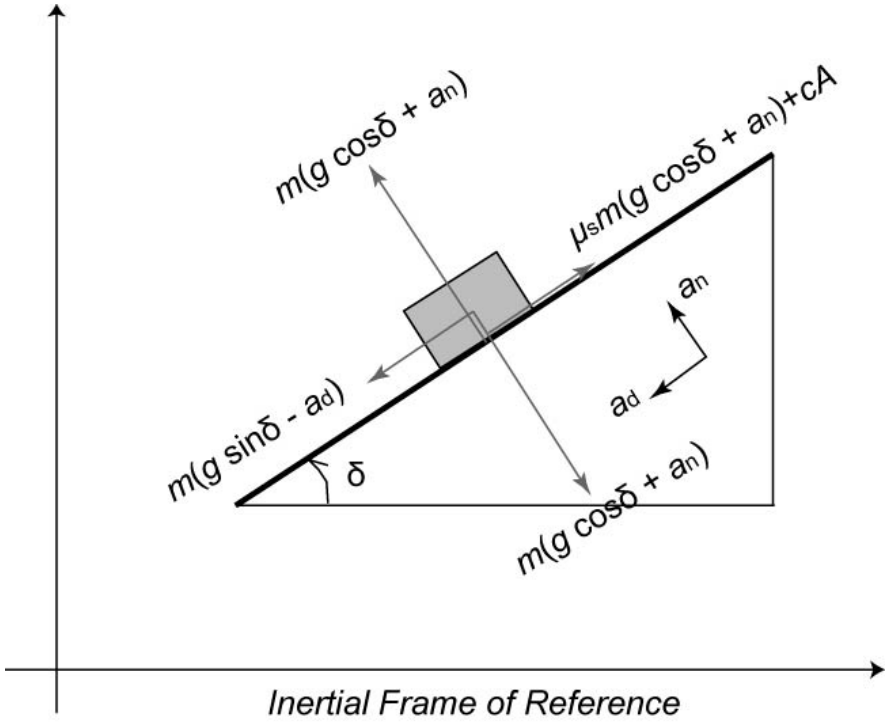

Fig.5 Free Landslide Body Diagram about Mountain Body under Earthquake Ground Motion and Critically Balanced Conditions ([8] was simplified)

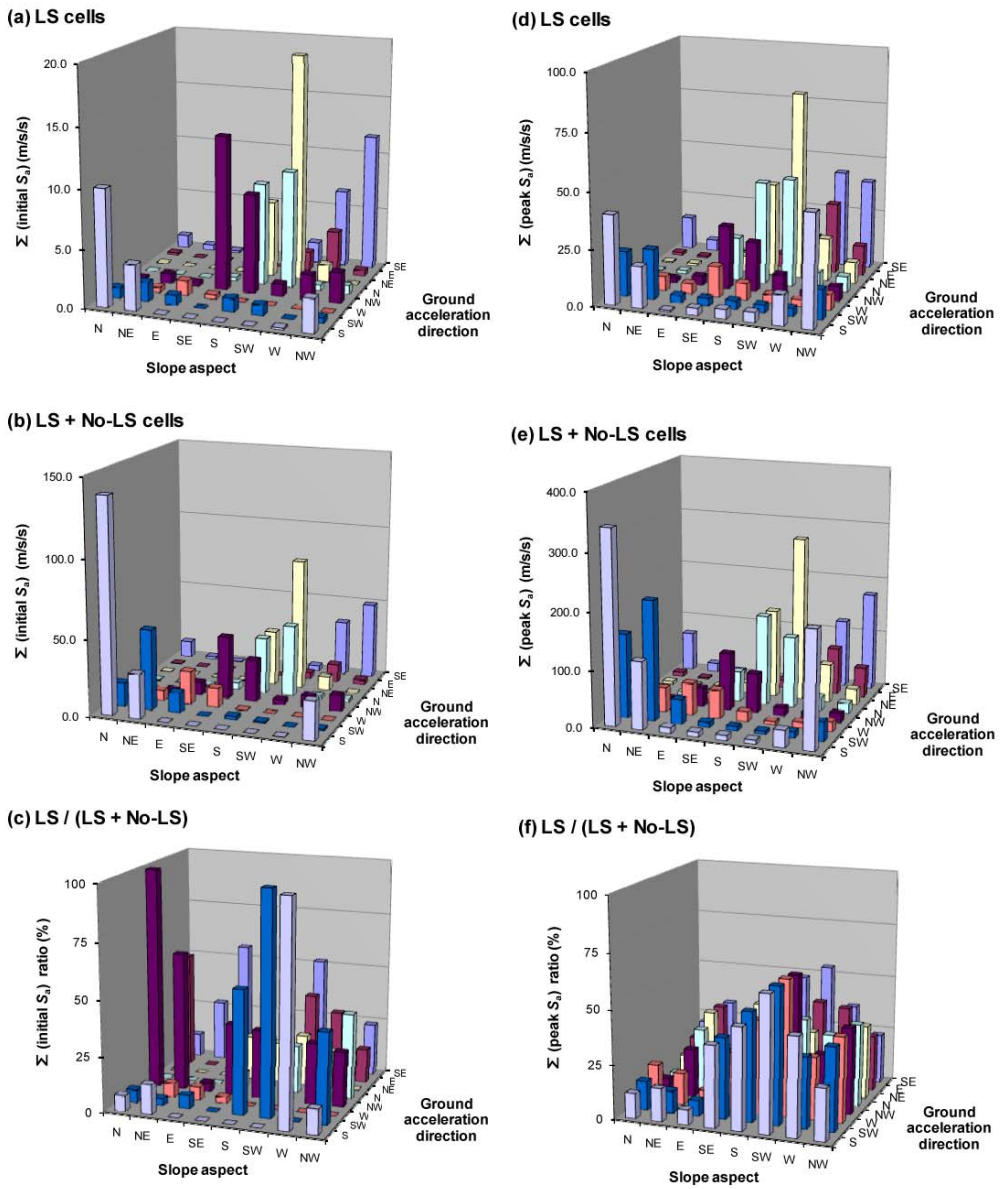

Fig.6 Accumulated Initial Sliding Acceleration (ISA) between Slope Aspects and Ground Acceleration Direction in (a) 2,072 Landslide Cells, (b) Whole Cells (2,072 Landslide Cells + 54,289 No-landslide Cells), (c) Normalized Accumulated ISA. Accumulated Peak Sliding Acceleration in (d) 2,072 Landslide Cells, (e) Whole Cells, (f) Normalized Accumulated PSA.